AFRL-PR-WP-TP-2006-274

SIMULATING INLET DISTORTION EFFECTS IN A DIRECT-CONNECT SCRAMJET COMBUSTOR (POSTPRINT)

Mark R. Gruber, Mark A. Hagenmaier, and Tarun Mathur

JULY 2006

Approved for public release; distribution is unlimited.

STINFO COPY

PROPULSION DIRECTORATE
AIR FORCE MATERIEL COMMAND
AIR FORCE RESEARCH LABORATORY
WRIGHT-PATTERSON AIR FORCE BASE, OH 45433-7251

REPORT DOCUMENTATION PAGE

Form Approved
OMB No. 0704-0188

1. REPORT DATE *(DD-MM-YY)*	2. REPORT TYPE	3. DATES COVERED *(From - To)*
July 2006	Conference Paper Postprint	06/01/2001 – 06/01/2006

4. TITLE AND SUBTITLE
SIMULATING INLET DISTORTION EFFECTS IN A DIRECT-CONNECT SCRAMJET COMBUSTOR (POSTPRINT)

5a. CONTRACT NUMBER
In-house

5b. GRANT NUMBER

5c. PROGRAM ELEMENT NUMBER
62203F

6. AUTHOR(S)
Mark R. Gruber and Mark A. Hagenmaier (AFRL/PRAS)
Tarun Mathur (Innovative Scientific Solutions, Inc.)

5d. PROJECT NUMBER
3012

5e. TASK NUMBER
AI

5f. WORK UNIT NUMBER
00

7. PERFORMING ORGANIZATION NAME(S) AND ADDRESS(ES)

Propulsion Sciences Branch (AFRL/PRAS)
Aerospace Propulsion Division
Propulsion Directorate
Air Force Research Laboratory, Air Force Materiel Command
Wright-Patterson Air Force Base, OH 45433-7251

Innovative Scientific Solutions, Inc.
2766 Indian Ripple Road
Dayton, OH 45440

8. PERFORMING ORGANIZATION REPORT NUMBER
AFRL-PR-WP-TP-2006-274

9. SPONSORING/MONITORING AGENCY NAME(S) AND ADDRESS(ES)

Propulsion Directorate
Air Force Research Laboratory
Air Force Materiel Command
Wright-Patterson AFB, OH 45433-7251

10. SPONSORING/MONITORING AGENCY ACRONYM(S)
AFRL-PR-WP

11. SPONSORING/MONITORING AGENCY REPORT NUMBER(S)
AFRL-PR-WP-TP-2006-274

12. DISTRIBUTION/AVAILABILITY STATEMENT
Approved for public release; distribution is unlimited.

13. SUPPLEMENTARY NOTES
Conference paper published in the 42nd AIAA/ASME/SAE/ASEE Joint Propulsion Conference & Exhibit (2006).

The U.S. Government is joint author of the work and has the right to use, modify, reproduce, release, perform, display, or disclose the work. PAO Case Number: AFRL/WS 06-1463; Date cleared: 09 Jun 2006. Paper contains color.

14. ABSTRACT

Direct-connect simulations of scram jet combustors typically use facility nozzles designed to produce uniform flow entering the test article. Conversely, in free-jet and flight experiments, where air is ducted to the supersonic combustor through an inlet, flow entering the test article will be inherently distorted. These distortion effects can include non-uniform boundary layer thicknesses on the walls and relatively strong oblique shock waves. In this work, a special piece of hardware (called a distortion generator) was designed to mimic the effects of inlet distortion in a direct-connect test environment. The design methodology for this distortion generator will be described along with details of its fabrication and installation into the experimental research facility. Finally, the results of computational and experimental calibrations will be presented. These results confirm that distortion characteristics anticipated in freejet and flight experiments can be effectively simulated in the direct-connect test environment. This new hardware will enable future experimental investigations aimed at understanding the effects of inlet-induced distortion on combustor operability and performance.

15. SUBJECT TERMS
Supersonic combustion ramjet, direct-connect testing, computational fluid dynamics

16. SECURITY CLASSIFICATION OF:			17. LIMITATION OF ABSTRACT:	18. NUMBER OF PAGES	19a. NAME OF RESPONSIBLE PERSON (Monitor)
a. REPORT	b. ABSTRACT	c. THIS PAGE			Mark R. Gruber
Unclassified	Unclassified	Unclassified	SAR	18	19b. TELEPHONE NUMBER *(Include Area Code)* N/A

Standard Form 298 (Rev. 8-98)
Prescribed by ANSI Std. Z39-18

42nd AIAA/ASME/SAE/ASEE Joint Propulsion Conference & Exhibit
9 - 12 July 2006, Sacramento, California

AIAA 2006-4680

Simulating Inlet Distortion Effects in a Direct-Connect Scramjet Combustor

Mark R. Gruber* and Mark A. Hagenmaier†
Air Force Research Laboratory, WPAFB, Ohio, 45433

and

Tarun Mathur‡
Innovative Scientific Solutions, Inc., Dayton, Ohio, 45440

A special piece of hardware (called a distortion generator) was designed using computational tools to mimic the effects of inlet distortion in a direct-connect test environment. Direct-connect simulations of scramjet combustors typically use facility nozzles designed to produce uniform flow entering the test article. However, in free-jet and flight experiments, where air is ducted to the supersonic combustor through an inlet, flow entering the test article will be inherently distorted. These distortion effects can include non-uniform boundary layer thicknesses on the walls and relatively strong oblique shock waves. In this work, the design methodology for the distortion generator is described along with details of its fabrication and installation into the experimental research facility. Finally, the results of computational and experimental calibrations are presented. Results confirm that distortion characteristics anticipated in freejet and flight experiments can be effectively simulated in the direct-connect test environment. This new hardware will enable future experimental investigations aimed at understanding the effects of inlet-induced distortion on combustor operability and performance.

Nomenclature

A	=	cross-sectional area
H	=	engine throat height
P	=	static pressure normalized by 1-D static pressure at the engine throat
P_P0	=	combustion heater total pressure
T_VH	=	combustion heater total temperature
W	=	mass flow rate
X	=	streamwise coordinate normalized by facility nozzle exit height (X=0 at engine throat)
Y	=	transverse coordinate normalized by facility nozzle exit height (Y=0 at cowl wall)
Z	=	spanwise coordinate normalized by facility nozzle exit height (Z=0 at spanwise centerline)

I. Introduction

DEVELOPMENT of supersonic combustion ramjet (scramjet) engines commonly involves several phases of experimental evaluation in close collaboration with computational fluid dynamics (CFD) simulations. Generally, component-level experiments are conducted in free-jet (for inlet-isolator components) and direct-connect (for isolator-combustor components) facilities, while the integrated engine (inlet-isolator-combustor-nozzle) is evaluated in a free-jet facility prior to flight testing.

In the direct-connect test environment, scramjet combustor simulations are typically accomplished using a facility nozzle that is designed to produce a uniform, supersonic gas stream with one-dimensionally averaged flow properties that match the expected conditions at the engine throat (entrance to the engine isolator) in a flight vehicle.

---

* Senior Aerospace Engineer, Propulsion Directorate, AFRL/PRAS, 1950 Fifth Street, Associate Fellow.
† Senior Aerospace Engineer, Propulsion Directorate, AFRL/PRAS, 1950 Fifth Street, Senior Member.
‡ Senior Research Engineer, 2766 Indian Ripple Road, Senior Member.

While this test environment offers substantial advantages over the free-jet environment (reduced experimental complexity, potentially longer test duration, generally simplified test article design constraints, more flexible instrumentation options, etc.), direct-connect testing does not reproduce the highly distorted flow profile caused by oblique shocks generated in the scramjet inlet. This raises concerns that the performance and operability results obtained in direct-connect experiments may not be representative of the free-jet and/or flight environments.

Distortion effects have been studied in traditional direct-connect testing by mounting a small compression ramp on one wall to generate a shock representing the cowl-lip shock that would exist in a full engine. However, this approach also generates a strong expansion fan at the end of the ramp. This expansion fan weakens the shock generated by the ramp, resulting in an inaccurate simulation of the true distortion that would be generated in the inlet. The approach used in the current investigation is a non-traditional form of direct-connect testing, where a facility nozzle is used to generate the average conditions at a plane upstream of the engine throat where the conditions in the full engine are nearly uniform. Starting at this plane, the full engine geometry is replicated, causing the shocks generated within the direct-connect hardware to be consistent with those in the full engine. It is important to note that in both traditional and non-traditional direct-connect testing, the boundary layer characteristics may not adequately match those that exist in the full engine. Boundary layer modification (e.g., bleed, mass injection, or vortex generators) may be used to improve the match; none of these approaches is explored in the current work.

This work began with the desire to experimentally examine the effects of inlet distortion on the performance and operability of an isolator-combustor model in the direct-connect combustion research laboratory at the Air Force Research Laboratory (AFRL). As mentioned above, this environment offers advantages in assessing the scramjet isolator-combustor, but its most notable shortfall is that the inflow to the model is a uniform supersonic stream. In this work, a methodology for designing a special piece of hardware (called a distortion generator) was sought to simulate the effects of inflow distortion in this research facility. If successful, this modification to the traditional direct-connect test approach would provide valuable information on flowpath performance and operability earlier in the scramjet engine development process. This paper describes various aspects of the development of the distortion generator, including the design methodology, the fabrication and installation of the hardware, and the results of flowfield calibrations. Comparisons are made between computational and experimental results.

II. Design of an Inflow Distortion Generator

A. Design Approach

In a planar or 2-D inlet with a flat cowl, the internal flowfield is dominated by a single oblique shock that is generated by the flow turning at the cowl leading edge, as shown in Figure 1. Neglecting the boundary layers, the flow is nearly uniform at each station where that oblique shock reflects off the walls. At the first reflection point (where the shock hits the body surface), flow is parallel to the cowl surface. At the second reflection point (where the shock hits the cowl surface), flow is parallel to the body surface. Depending on the length of the internal compression section and the shock angle, more reflections may occur upstream of the engine throat. Any of these shock-reflection locations could be selected as the start of the distortion generator. The advantage of the first reflection point in Figure 1 is that the flow is parallel to the cowl. Beginning the distortion generator at this point would yield a piece of hardware mounted parallel to the cowl, which is consistent with the traditional direct-connect operation without distortion. The advantage of the second reflection point is that the flow suffers fewer total

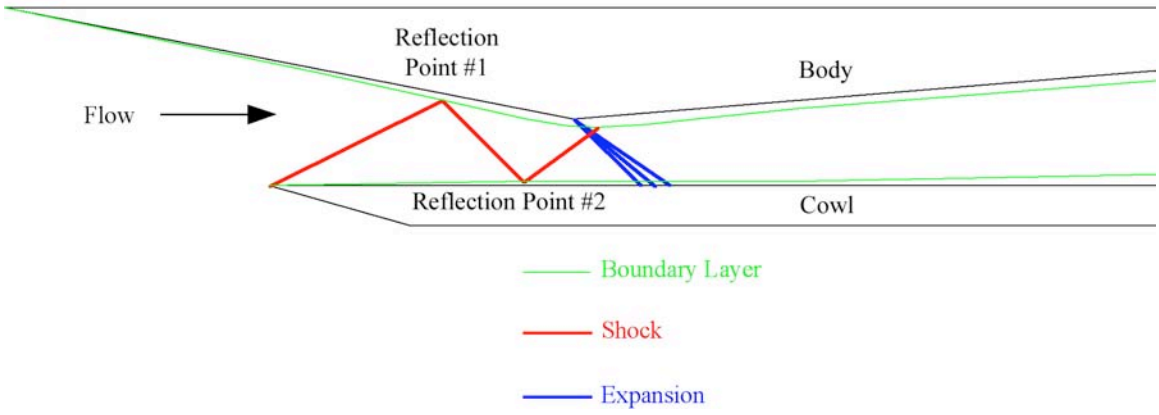

Figure 1. Scramjet internal flow structure.

pressure losses between that point and the engine throat and therefore requires a lower facility pressure to produce the same conditions at the throat. However, in this case, either the test article or the inflow hardware would have to be rotated to align the flow exiting the distortion generator with the body surface. For the present study, the first reflection point was selected as the location to begin the distortion generator. The following four-step process was employed in the computational design of the distortion generator:

- **Step 1**: For the flight condition of interest, the shock reflection locations for the full engine were identified, using a 2-D turbulent CFD analysis. The Mach number and flowpath height at the reflection point selected as the "match-point" were also determined.
- **Step 2**: A facility nozzle was designed using traditional method-of-characteristics procedures to generate the Mach number and match-point height identified in Step 1. From the match-point height and Mach number, the throat height was determined. In the present work, two expansion sections were designed to provide additional flexibility. The first section expands the flow from the nozzle throat height to the engine throat height, resulting in a facility nozzle that can be connected either to the second expansion section or directly to the engine throat. The second section expands the flow from the engine throat height to the match-point height. This section is then combined with the vehicle geometry from the match-point location to the engine throat to define the distortion generator. This device has equal inflow and outflow areas.
- **Step 3**: For tunnel conditions consistent with the total conditions expected at the chosen reflection point, 3-D turbulent CFD analysis was performed to evaluate the distortion produced by the distortion generator. This CFD analysis accounted for various effects (variable specific heats, and viscous effects) that were not accounted for in the MOC design tool.
- **Step 4**: The design was adjusted as necessary to improve the match between the distortion produced by the distortion generator and the distortion present in the full engine. Possible adjustments included shifting the match-point location, adjusting the nozzle throat height, or modifying the boundary layer thickness (via bleed, mass injection, etc.).

All viscous CFD calculations performed in this work, both the 2-D flight condition analysis and the 3-D distortion generator analysis, were performed with the CFD++ tool from Metacomp Technologies.[1] CFD++ has been demonstrated for many high-speed propulsion applications.[2-8] The fluid was modeled as a mixture of thermally-perfect gases, and turbulence was modeled using the cubic k-epsilon model. Structured grids were generated with the Gridgen tool from Pointwise. Maximum cell size in all directions was approximately 0.1 inch, with clustering near the walls to provide adequate resolution of the boundary layers. In all configurations simulated, the design is symmetric from left to right. This symmetry was enforced within the CFD, allowing a factor of two reduction in the required number of computational cells. The grid included a slightly divergent isolator with a length of approximately 12H, followed by a higher divergence section with a length of approximately 6H. The section with higher divergence was included to allow flow reattachment for back-pressured simulations, making the outflow boundary condition well-posed.

B. Design Results and Implementation

The aerodynamic contour of the distortion generator that resulted from the design approach described above is shown in Figure 2. This contour served as the basis for the design and fabrication of a hardware section for experimental evaluation. The expansion region required to accelerate the facility nozzle outflow to conditions encountered at the first shock reflection point comprises over half the length of the contour. The compression surface begins at approximately X = -5 and the cowl wall was held flat throughout.

Table 1 shows the configuration matrix used in the present investigation. Based on the available experimental hardware, two traditional direct-connect arrangements were assembled (Configurations 1 and 2) in addition to the arrangement based on the distortion generator (Configuration 3). In Configuration 1, a Mach 2.56 nozzle was installed without a facility isolator. Configuration 2 used a Mach 2.70 facility nozzle with a 7.2H long facility isolator of constant cross-sectional area. Finally, in Configuration 3, a Mach 2.84 facility nozzle was used upstream of the distortion generator. Figure 3 contains schematics of these three arrangements along with a representation of the body wall of a flight vehicle inlet. In these schematics, the flow direction is from left to right. In the two typical direct-connect experimental arrangements, the supersonic flow entering the test article (engine isolator + combustor) is designed to be free of shock waves and have uniform properties in the core flow. The main difference between these two configurations should be the boundary layer properties entering the engine. The hardware downstream of the engine throat (X = 0) is common to all configurations.

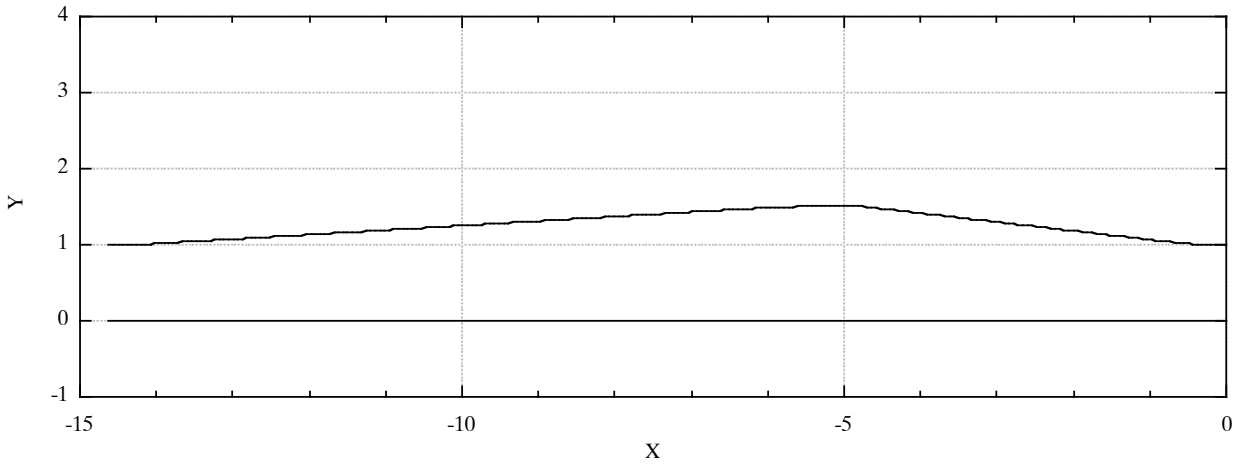

Figure 2. Aerodynamic contour of distortion generator.

Table 1. Hardware configuration matrix.

Configuration	Facility Nozzle	Facility Isolator	Distortion Generator	Engine Isolator
1	2.56	No	No	Forward
2	2.70	Yes	No	Forward
3	2.84	No	Yes	Forward

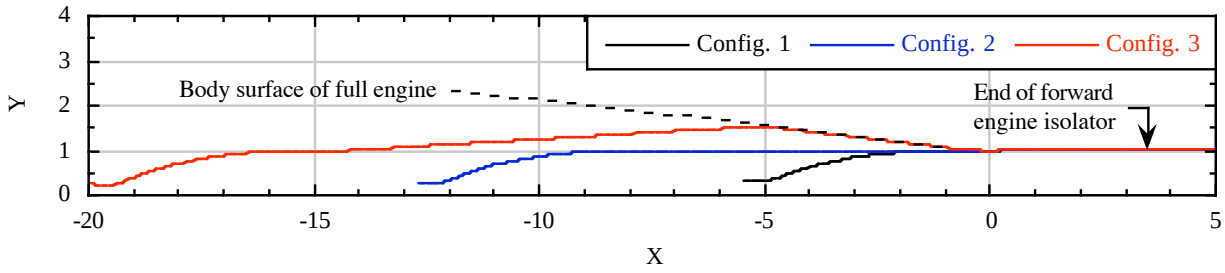

Figure 3. Hardware configurations for clean flow and distorted flow studies.

This distortion generator design was originally developed for a Mach 6.5 flight condition that had an estimated throat Mach number of 3.25. The design process led to a facility nozzle that produced a Mach number of approximately 3.60. After passing through the distortion generator, the average Mach number was approximately 3.25, and the pressure distortion was similar to that predicted for the full engine in flight, as shown in Figure 4. After the distortion generator was designed for these conditions, the research direction changed to focus on lower-speed applications. The distortion generator was re-evaluated to determine its suitability for the new conditions. Results indicated that the use of an existing Mach 2.84 facility nozzle with the "as designed" distortion generator would provide a suitable level of distortion, and a similar average Mach number to the conditions anticipated at the lower-speed. Figure 5 presents computational results from the three hardware configurations of interest. This plot shows that the one-dimensional Mach number achieved at the engine throat and at the exit of the forward engine isolator is only slightly dependent on the hardware configuration. The engine throat Mach number is expected to vary only ±0.1 across the three hardware configurations.

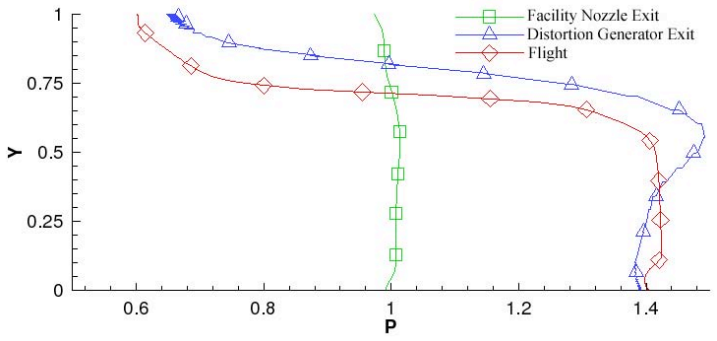

Figure 4. Predicted pressure profiles for two ground test approaches and for flight.

III. Experimental Resources

A continuous flow of air at up to 30 lbm/sec, 750 psia, and 1660°R, with 3.0 psia continuous exhaust, can be provided to the laboratory by the Research Air Facility. This facility uses an in-stream combustion heater (fueled with compressed natural gas) to generate conditions suitable for simulations of Mach 3.5 – 7.0 flight conditions. Liquid and gaseous oxygen systems are available for providing make-up oxygen to the combustion-heated air stream. Liquid and gaseous hydrocarbon fuel systems deliver fuel to the research combustor. An electric fuel heater heats combustor fuel to the required temperatures for various combustor simulation conditions. A recirculating cooling water system provides 2500 gpm at 70 psia; raw dump water at 350 psia is also available. The entire flowpath is secured to a thrust stand for direct measurements of the thrust generated by the combustor. This measurement may be combined with wall static pressure measurements and a performance analysis routine to deduce combustion efficiency and other performance parameters. Additional details about the facility, including the available instrumentation and fuel heater, are presented elsewhere.[9]

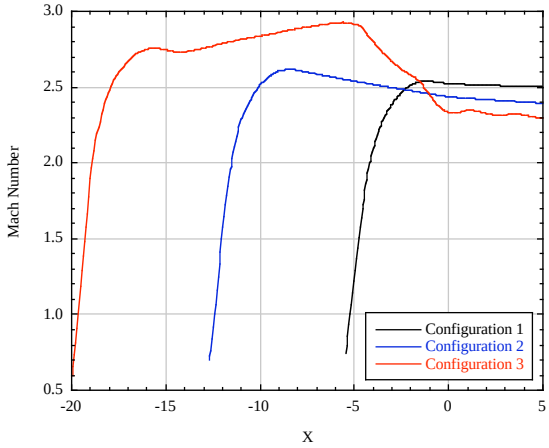

Figure 5. Axial distribution of one-dimensional Mach number for each hardware configuration.

A. Distortion Generator Mechanical Design and Fabrication

Figure 6 shows the assembly drawings for the distortion generator. The flowpath section was comprised of four walls (two side walls, a body wall, and a cowl wall). The body wall contained the expansion and compression surfaces required to generate the desired distorted flow profile; the other three walls were flat. Each wall was a composite assembly of oxygen-free copper brazed to a stainless steel support structure. Passages were milled into the copper to allow cooling water to be delivered and routed through the walls. The cooling-water flowed in the streamwise direction within the two side walls and in the spanwise direction within the body and cowl walls. Water supply and return ports were welded to the stainless steel support structure. Figure 6 shows the cooling water ports on the cowl wall.

Twenty-nine instrumentation ports were provided in the cowl wall. These ports could be used for either wall static pressure or wall temperature measurements. The ports were positioned between the cooling channels in the cowl wall and were primarily located on the spanwise centerline of the flowpath, but off-centerline taps were also

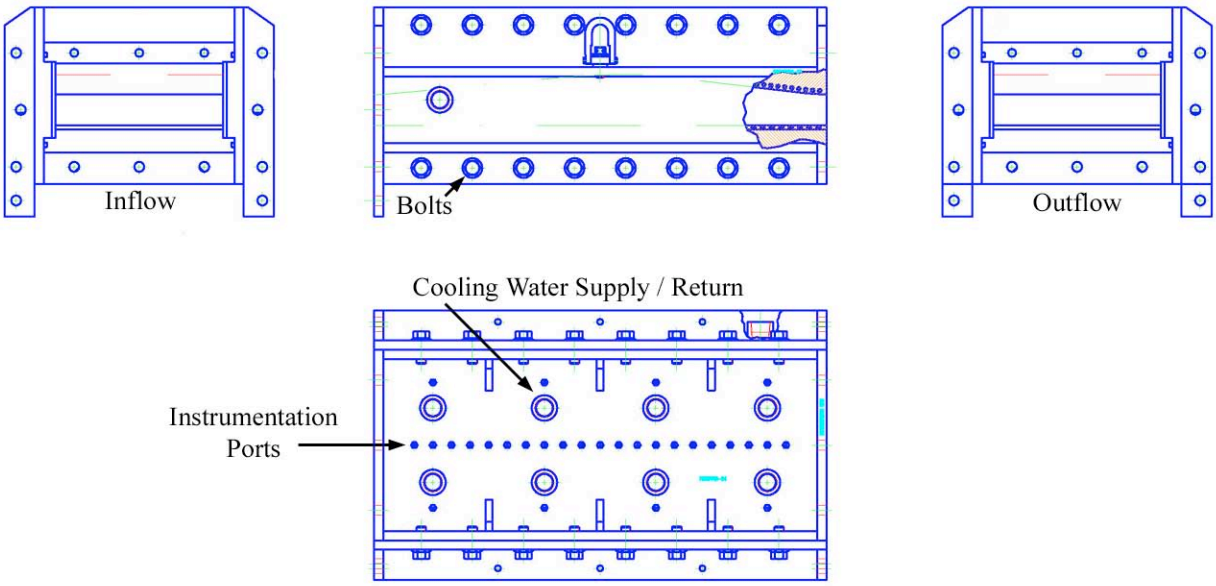

Figure 6. Distortion generator assembly drawing.

available at four axial positions. Figure 6 shows the instrumentation layout.

The four-wall assembly was bolted together. The mating surfaces of the walls were sealed using silicon O-ring cord (0.210-in. diameter). Upstream and downstream flanges allowed the assembled component to be attached to the facility nozzle and the engine isolator; the flange seals were also made with silicon O-rings (0.210-in. diameter). Figure 6 shows the bolts in the side view of the assembly.

B. Flowpath Calibration

The flowfields associated with the various nozzle and isolator combinations shown in Figure 3 were studied experimentally using wall pressure measurements and in-stream probe-based measurements. The number of wall pressure measurements varied depending on the hardware configuration in use. Configuration 1 had 38 instrumented pressure taps while Configurations 2 and 3 had 66 and 63, respectively.

A 6-element water-cooled traversing probe (shown in Figure 7) was traversed into the flowfield to document in-stream properties. The probe ports were spaced 0.25-in. apart such that an effective width of 1.25-in. could be spanned. The two outer probe ports were dedicated to total temperature measurements (0.125-in. OD aspirated ceramic tips surrounding Type-B thermocouple junctions). The four inner probe ports were used to measure pitot pressure. Each port consisted of a 0.035-in. OD tube mounted concentrically within a 0.062-in. OD tube. The annulus between these tubes was supplied with spray water. Pitot pressure was sensed using the smaller tube; each of the smaller tubes was connected to an Omegadyne PX5500L1 pressure transducer (500 psia or 1000 psia) through a length of 0.062-in. diameter nylon tubing. The probe was installed into a specially designed housing that had a modular inlet flange allowing it to be smoothly mated to either the nozzle exit or the exit of the forward isolator. The spray-cooled housing had three probe attachment ports – one on top and one on each side. This allowed the probe to be traversed from top-to-bottom across the entire duct height at the spanwise centerline, or from either side wall to a point approximately 3.5 in. into the flow. The exit of the housing mated to an 8-in. carbon steel pipe that interfaced with the facility exhaust.

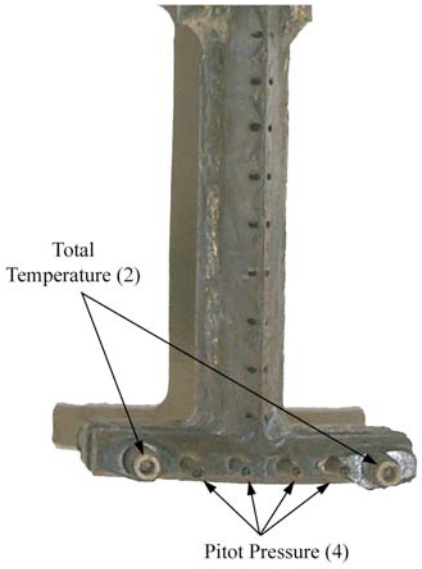

Figure 7. Photograph of calibration probe.

IV. Results

In the following sections, various computational and experimental results will be presented. Each of the three hardware configurations was experimentally evaluated at a variety of test conditions. For brevity, results from only select conditions will be presented in this paper. Comparisons will be made between the experimental and computational results where appropriate. Finally, additional computational results will be shown to provide details of the clean and distorted flow profiles beyond what is inferred from the physical measurements.

A. Experimental and Computational Comparisons

1. Configuration 1

Figure 8 shows the measured and predicted wall static pressure distributions through the facility nozzle and forward engine isolator used in Configuration 1 for a case with P_P0 = 185 psia and T_VH = 2500°R. In this case, the measured pressure distribution compares favorably with the computational results. A slight discrepancy occurs in the experiments within the forward engine isolator. This hardware section has a thermal barrier coating applied to the walls that results in an abrupt change in wall heat transfer and surface roughness. The effect of these influences is to elevate the wall pressure slightly as observed in the experimental measurements.

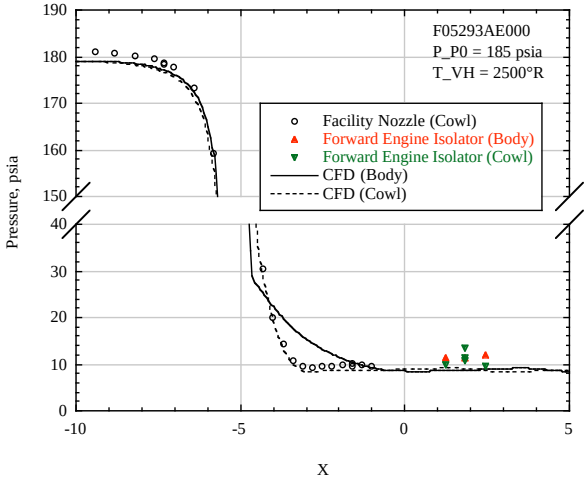

Figure 8. Wall static pressure distributions from Configuration 1.

Figure 9 contains pitot pressure and total temperature data from the exits of the facility nozzle (Figure 9a) and forward engine isolator (Figure 9b). Note that in the physical measurements, the thermocouples are positioned ±0.625-in. off the centerline and the pitot probes are ±0.125- and ±0.375-in. off the centerline while the computational results are from the centerline. In general, the agreement between the computation and the experiment is very good although there are some discrepancies. The computation predicts thinner thermal boundary layers than observed in the measurements. The body side boundary layer (near Y = 1.0) as inferred from the pitot pressure data is also thinner in the computational simulation than in the experiment. Finally, a feature peculiar to the experiment is observed near Y = 0.6; this feature is common to the experiments where the calibration probe is used and is attributed to probe-induced interference. Aside from these features, the profiles show a relatively uniform core flow over the majority of the duct height at both axial locations. This is consistent with the traditional direct-connect experimental approach.

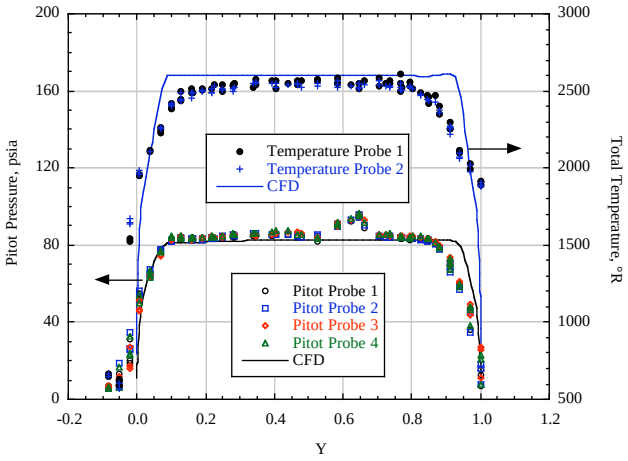

(a) Facility nozzle exit.

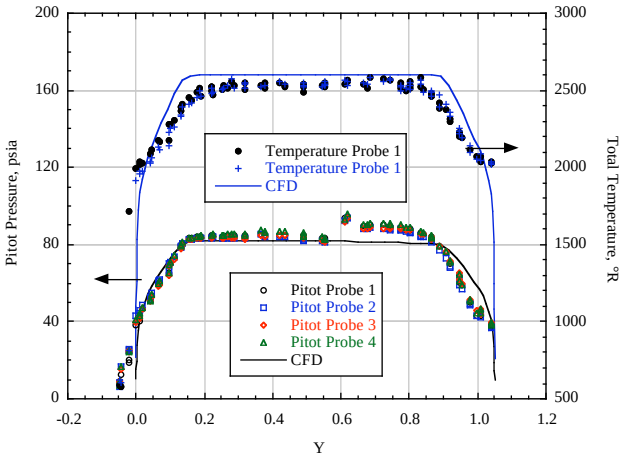

(b) Forward engine isolator exit.

Figure 9. Pitot pressure and stagnation temperature profiles from Configuration 1.

2. Configuration 2

Wall pressure distributions from Configuration 2 are presented in Figure 10 for a case where P_P0 = 225 psia and T_VH = 2000°R. Excellent agreement is obtained between the physical measurements and the computational results, especially through the facility nozzle and facility isolator sections. As noted in the experimental results from Configuration 1, the two data sets diverge slightly in the forward engine isolator due to the influence of the thermal barrier coating on the walls of that hardware.

Pitot pressure and total temperature profiles from Configuration 2 appear in Figure 11. Measurements and computations agree relatively well at the facility nozzle exit plane (Figure 11a). The experimental pitot pressure data again show the presence of a probe-induced disturbance (near Y = 0.55). Boundary layer behavior appears well predicted at this axial position, although the total temperature measurements near the cowl wall appear artificially high. At the exit of the forward engine isolator (Figure 11b), the total temperature measurements near the cowl wall exhibit similar behavior. At this station, it is clear that the wall boundary layers have thickened noticeably because of the facility isolator. The region of uniform flow in the core of the flowpath is greatly reduced compared with the results from Configuration 1. Also, the pitot pressure measurements in the core suggest a local region of higher Mach number (lower pitot pressure values) compared with the CFD result. Aside from these differences, Configuration 2 appears to produce a clean supersonic flow with substantially thicker boundary layers than were observed in Configuration 1. Since

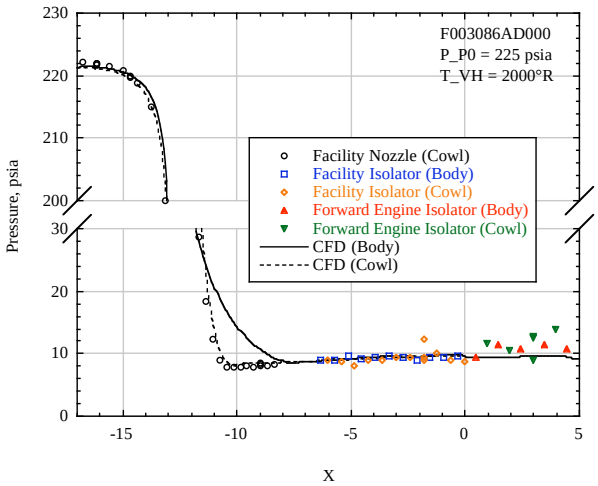

Figure 10. Experimental and computational wall static pressure distributions from Configuration 2.

both hardware assemblies also generate approximately the same one-dimensional engine throat Mach number (see Figure 5), isolator-combustor experiments using these configurations should reveal the influences of wall boundary layer thickness on engine performance and operability.

3. Configuration 3

Wall static pressure data through the various hardware sections that comprise Configuration 3 are shown in Figure 12. Both experimental and computational data from a case where P_P0 = 250 psia and T_VH = 2500°R are included in this figure for comparison. Excellent agreement is observed between the two data sets suggesting that the behavior of the distortion generator is well predicted by CFD. The wave generated by the body side compression surface intersects the cowl wall at the same axial position in the experiment and the simulation (near X = -2). The behavior of the reflected shock wave also compares well, although the peak pressure measured in the experiment (near X = 2) is slightly higher than predicted. The expansion on the cowl wall is also very well predicted (0 < X < 3). As observed in the other two configurations, this elevated pressure may be related to the presence of the thermal barrier coating on the forward engine isolator walls.

Figure 13 shows comparisons between the experimental and computational in-stream measurements. In these plots, probe measurements and computational results are presented from the spanwise centerline. The physical measurements were made in the same locations as in the previous configurations. The data shown in Figure 13a from the facility nozzle exit exhibit relatively good agreement between the measurements and predictions, although the thermal boundary layers are somewhat different. Both pitot pressure and total temperature distributions reveal a uniform core flow over the majority of the duct height. A slight probe-induced disturbance is present near Y = 0.55 that is absent from the CFD results. At the exit of the forward engine isolator, the pitot pressure and total temperature distributions become substantially skewed due to the presence of the distortion generator (Figure 13b). Predictions and measurements again compare quite well except for the probe-induced disturbance near Y = 0.55.

Figure 14. shows three photographs of the flow surfaces within the forward engine isolator and the distortion generator. In each photograph, the engine throat location is noted along with the flow direction. Because the in-stream combustion heater used in these experiments generates a finite amount of small soot particles, visualization of shock wave patterns on the walls of various hardware components is possible. The soot particles tend to accumulate in regions of large

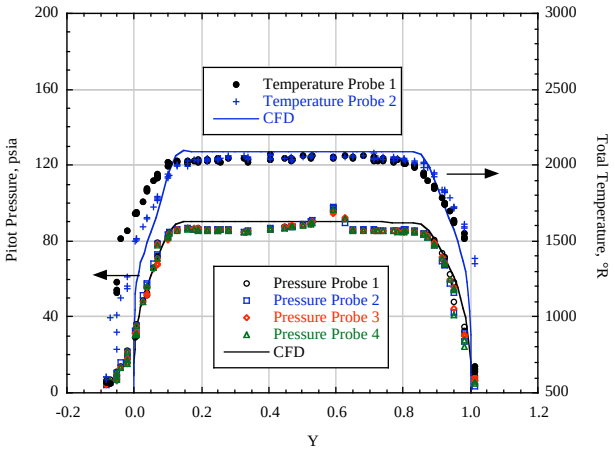

(a) Facility nozzle exit.

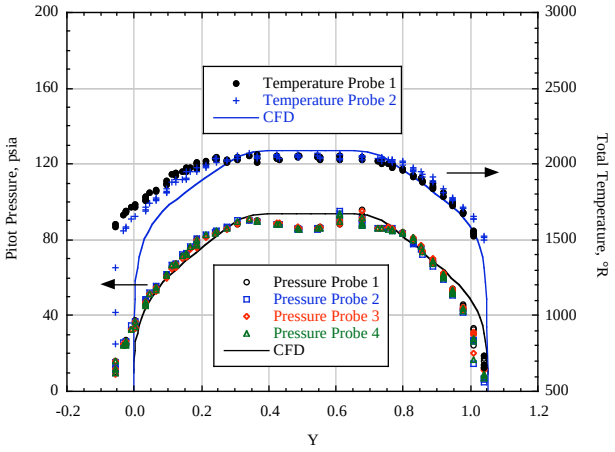

(b) Forward engine isolator exit.

Figure 11. Pitot pressure and stagnation temperature profiles from Configuration 2.

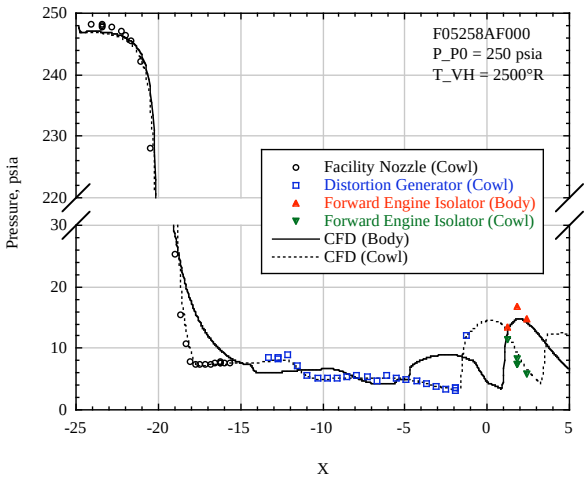

Figure 12. Experimental and computational wall static pressure distributions from Configuration 3.

pressure and velocity gradients leaving discernible evidence of shock footprints. Figure 14a shows a portion of the distortion generator with one of the side walls removed. The oblique shock wave generated from the compression surface is observed, as is the first reflection of this wave from the cowl surface. This reflected wave then interacts with the body wall inside the forward portion of the engine isolator (Figure 14b). A second reflected wave then interacts with the cowl wall (Figure 14c). As expected, the shock footprints suggest that the wave is relatively planar across the central portion of the flowpath while it curves upstream near the side walls.

Similar information is obtained from the CFD simulations of this flowpath. For example, wall static pressure distributions are also shown in Figure 14 for direct comparison with the photographs of the experimental hardware. In these plots, black lines are used to identify the shock wave locations. Excellent agreement in both position and shape of the four features is observed between the computational and experimental results.

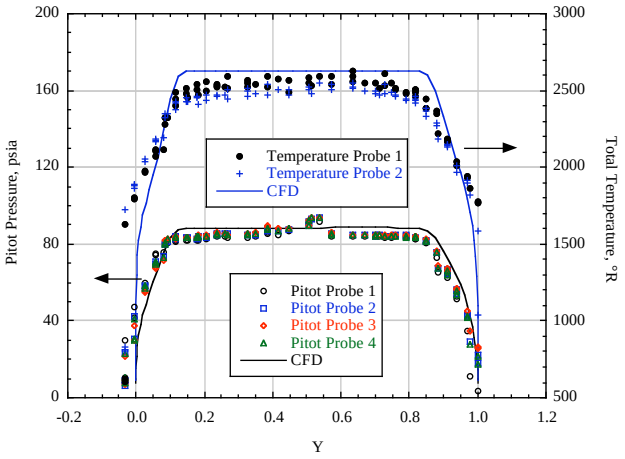

(a) Facility nozzle exit.

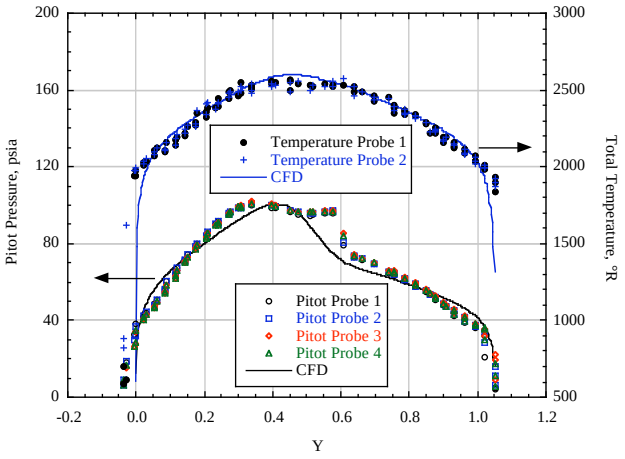

(b) Forward engine isolator exit.

Figure 13. Pitot pressure and stagnation temperature profiles from Configuration 3.

B. Computational Simulations with Elevated Back Pressure

Based on the excellent agreement between the experiments and computations during the calibration phase of this work, an additional CFD study was performed to investigate the impact of flow distortion on isolator and combustor performance. For this study, the outflow boundary condition was set to a fixed back pressure, such that the pressure ratio across the isolator was 4.5. This pressure ratio is representative of the isolator pressure ratio expected for flight Mach numbers of approximately 5.

The impact of inflow distortion on isolator performance is evaluated in terms of the position of the shock train within the isolator. The shock position is indicative of the amount of stability margin available to the engine. Figure 15 shows centerline pressure distributions, and Figure 16 shows centerline Mach number distributions. The pressure distributions show only a small change in the location of the start of the shock train as a function of hardware configuration. The Mach number distributions show that the two cases without distortion develop separated regions on the body and cowl walls at the same streamwise location. The configuration using the distortion generator, however, exhibits separation first on the cowl side. The separated region on the body side in this configuration is relatively small.

The impact of inflow distortion on combustor performance is evaluated by examining the mass flux distribution at the isolator exit plane. Differences in mass flux distribution may indicate that a different fuel injection pattern might be required for comparable combustor performance. Figure 17 shows the mass flux at the isolator exit for the three configurations of interest. The CFD indicates that, for each configuration, the majority of the air flow is pushed away from the side walls toward the center of the duct. Due to the larger separation on the cowl side, the configuration using the distortion generator also shows more mass being pushed toward the body side.

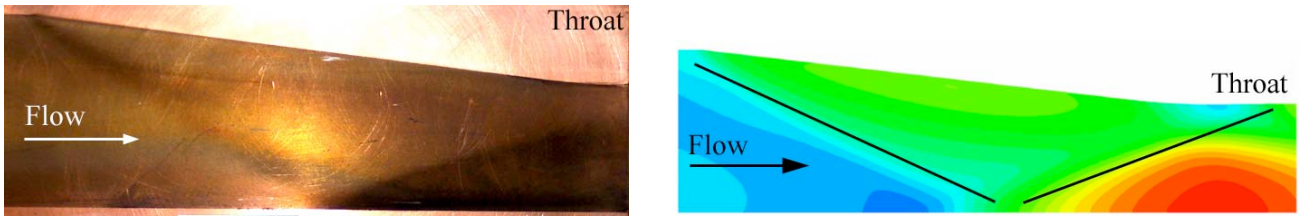

(a) Shock structure in distortion generator (side wall).

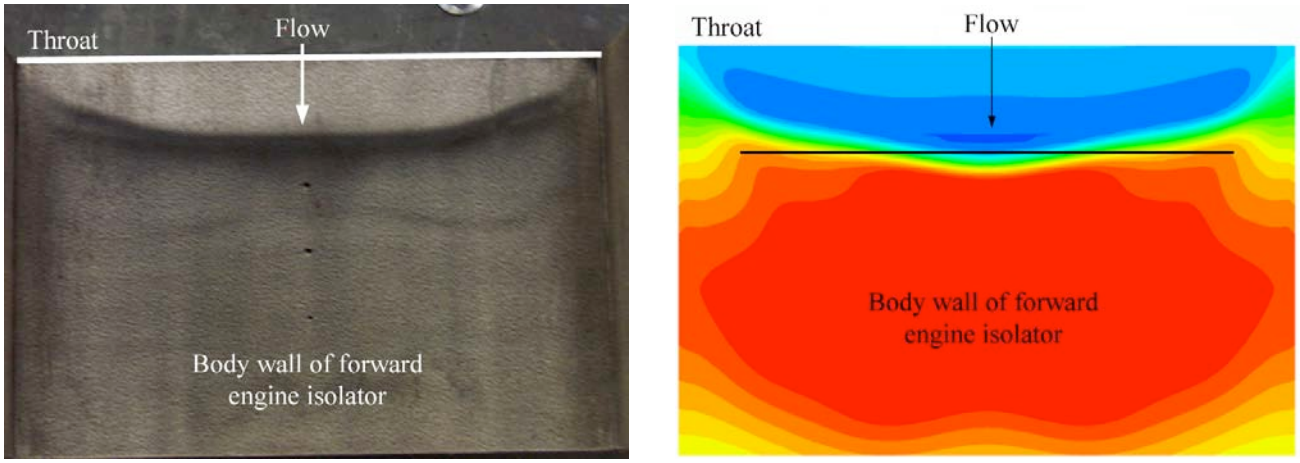

(b) Shock footprint on body wall of forward engine isolator.

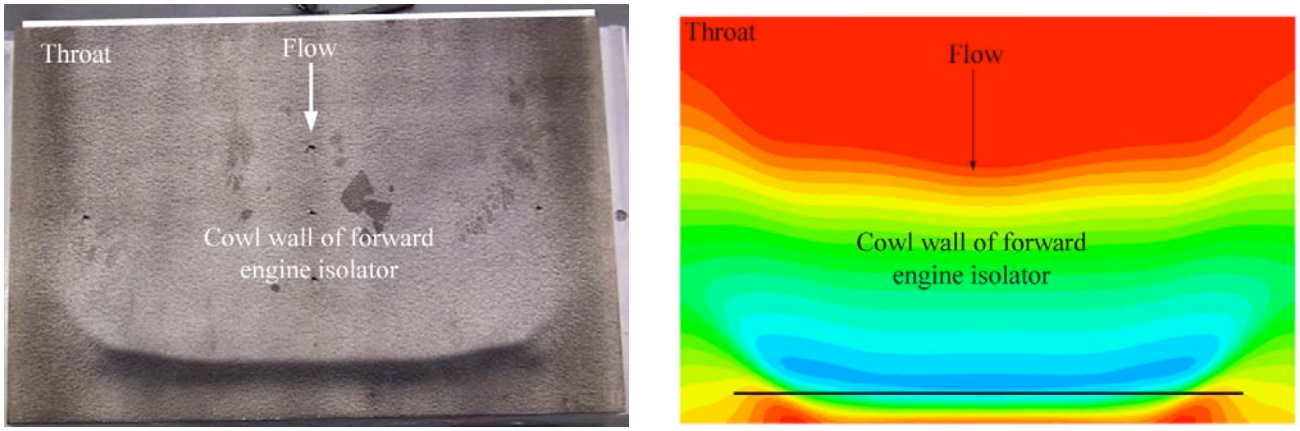

(c) Shock footprint on cowl wall of forward engine isolator.

Figure 14. Actual and predicted shock footprints on the walls of various hardware sections.

V. Future Work

Having established that both clean and distorted in-flow profiles of similar one-dimensional Mach numbers can be generated in the AFRL/PRAS direct-connect combustion facility, experimental assessments of the impacts of inflow distortion on the performance and operation of a dual-mode hydrocarbon-fueled scramjet will be conducted. Of particular interest are any changes to the combustor fuel distribution that may be required because of the non-uniform inflow mass distribution. Initially, the combustor performance and operability will be established using the Mach 2.56 facility nozzle with no facility isolator present (i.e., Configuration 1). These experiments will be conducted with gaseous hydrocarbon fuels. Following this characterization, Configuration 3 will be installed and the combustion experiments will be repeated. In addition, the symmetry assumption used in the current CFD results will be examined based on the results of related studies.[10]

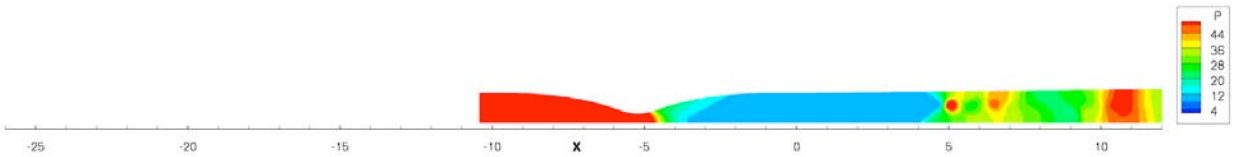

(a) Configuration 1.

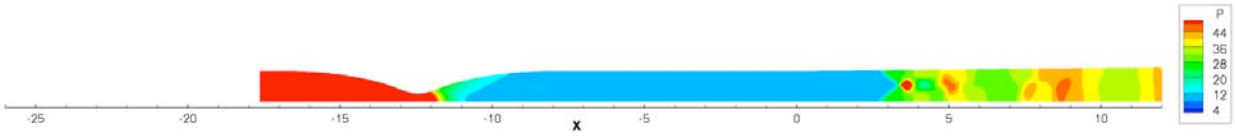

(b) Configuration 2.

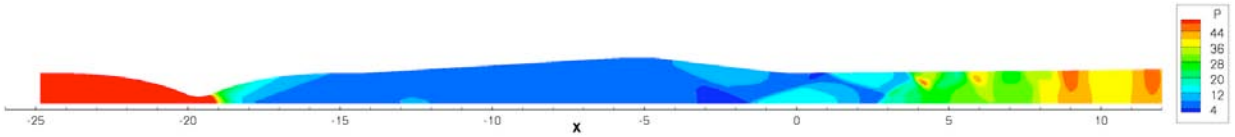

(c) Configuration 3.

Figure 15. Pressure distributions on spanwise centerline; isolator pressure ratio = 4.5.

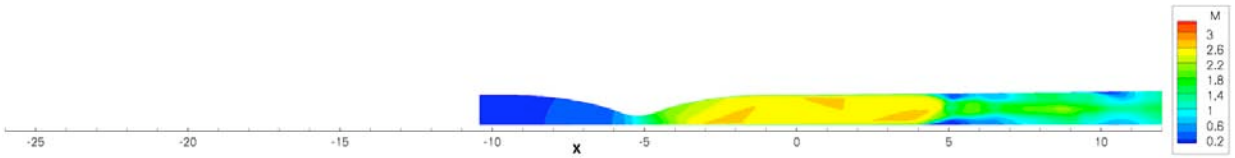

(a) Configuration 1.

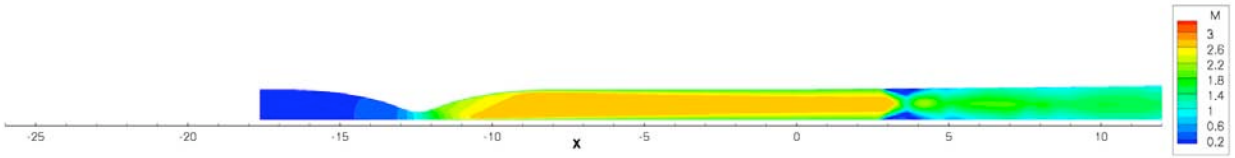

(b) Configuration 2.

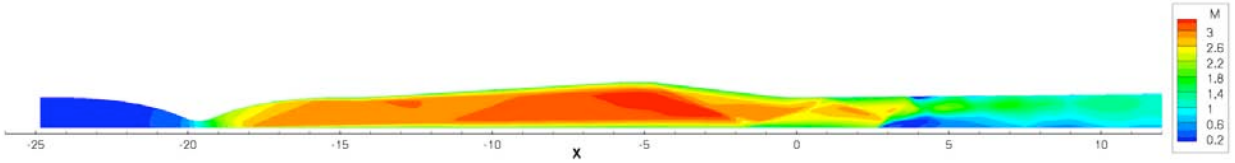

(c) Configuration 3.

Figure 16. Mach number distributions on spanwise centerline; isolator pressure ratio = 4.5.

VI. Conclusion

A novel approach to simulating inlet distortion effects in a direct-connect test environment was sought to investigate the effects of inflow distortion on combustor performance and operability. Computational fluid dynamics tools were used to design a new section of hardware, called a distortion generator, which would reproduce the shock structure encountered in a planar free-jet or flight vehicle inlet. This device expanded a clean supersonic flow to conditions at the first shock reflection point within the inlet. At this point, the distortion generator flow lines followed the inlet flow lines to the engine throat. This approach reproduced most of the features expected to be present in the inlet, with the exception of the boundary layers. Experimental and computational investigations were undertaken to calibrate the distortion generator and two other more traditional direct-connect hardware assemblies to evaluate their flow performance. Physical wall-based and in-stream measurements from the various configurations agreed relatively well with the results of computational simulations with a few minor discrepancies. The distortion

generator proved to operate effectively, and the flowfield it produced was substantially different from either of the flowfields generated by the more traditional direct-connect hardware. When simulated with elevated back pressure consistent with a Mach 5 combustion environment, the three hardware configurations were shown to generate similar mass flux distributions at the combustor inlet. Much of the air mass was directed toward the spanwise centerline of the flowpath in each configuration. However, in the case of the distortion generator, the air mass flux distribution was more skewed toward the body wall because of asymmetric boundary layer separation. This observation may have implications on how combustor fueling must be changed as a function of the level of inflow distortion. Future work will investigate the combustor operability and performance characteristics using these different hardware configurations to better assess the effects of inflow distortion in the direct-connect test environment.

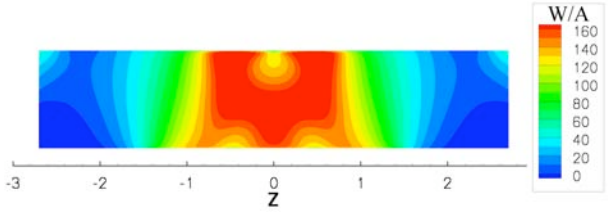

(a) Configuration 1.

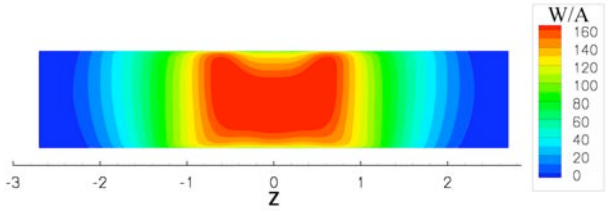

(b) Configuration 2.

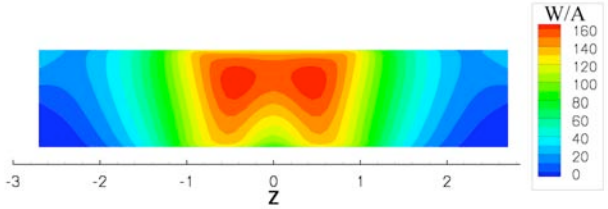

(c) Configuration 3.

Figure 17. Mass flux distributions at exit of engine isolator; isolator pressure ratio = 4.5.

Acknowledgments

The authors acknowledge the combined energies of the AFRL/PRA management (Mr. P. Buckley, Dr. T. Jackson, and Mr. R. Mercier) for their financial and technical support of this effort. The authors also acknowledge the help of Marty Haas of United Technologies Research Center, who provided the method-of-characteristics tool used for this effort. The computational resources for this project were provided by the DoD High Performance Computing Modernization Office at the ASC Major Shared Resource Center. Finally, the authors acknowledge the contributions of Mr. J. Diemer, Mr. W. Haendiges, Mr. R. Ryman, Mr. C. Smith, Mr. S. Smith, and Mr. G. Streby for technical and operational support of the experimental research facility. Support of the AFRL/PR Research Air Facility is also appreciated.

References

[1]Metacomp, http://www.metacomptech.com/index.html, 2005.

[2]Goldberg, U., Peroomian, O., Chakravarthy, S., Sekar, B., "Validation of CFD++ Code Capability for Supersonic Combustor Flowfields," AIAA Paper 1997-3271, July 1997.

[3]Hagenmaier, M. A., Tam, C.-J., and Chakravarthy, S., "Study of Moving Start Door Flow Physics for Scramjets," AIAA Paper 99-4957, November 1999.

[4]Hagenmaier, M. A., and Davis, D. L., "Scramjet Component Optimization Using CFD and Design of Experiments," AIAA Paper 2002-0544, January 2002.

[5]Grendell, K. M., "A Comparison Study of Rectangular and Chamfered Isolator Cross-Sectional Shape with Varied Divergence," AIAA Paper 2004-0129, January 2004.

[6]Brindle, A., Boyce, R. R., and Neely, A. J., "CFD Analysis of an Ethylene-Fueled Intake-Injection Shock-Induced-Combustion Scramjet Configuration," AIAA Paper 2005-3239, May 2005.

[7]O'Byrne, S., Stotz, I., Neely, A. J., Boyce, R. R., Mudford, N. R., and Houwing, A. F. P., "OH PLIF Imaging of Supersonic Combustion using Cavity Injection," AIAA Paper 2005-3357, May 2005.

[8]McGuire, J., Boyce, R., and Mudford, N., "Comparison of Computational and Experimental Studies on Shock Induced Ignition in Scramjets," AIAA Paper 2005-3394, May 2005.

[9]Gruber, M., Donbar, J., Jackson, K., Mathur, T., Baurle, R., Eklund, D., and Smith, C., "Newly Developed Direct-Connect High-Enthalpy Supersonic Combustion Research Facility," *Journal of Propulsion and Power*, Vol. 17, No. 6, 2001, pp. 1296-1304.

[10]Rodriguez, C. G., White, J. A., and Riggins, D. W., "Three-Dimensional Effects in Modeling of Dual-Mode Scramjets," AIAA Paper 2000-3704, July 2000.